A Re-examination of Ice Age Time Series

J. S. Reid

Ecofluidics Pty Ltd
P.O. Box 279
Cygnet
Tasmania
Australia 7112

jsr@ecofluidics.com
www.ecofluidics.com

September 2010

A Re-examination of Ice Age Time Series

Abstract

Since Milankovic (1941), it has been commonly assumed that the observed sequence of ice ages and interglacials of the last 430,000 years is driven by variations in solar insolation at high northern latitudes due, in turn, to variations in the Earth's orbital parameters. Here, data in the form of proxy temperature values from EPICA Dome C in Antarctica are re-examined using modern time series methods, and variance density spectra are plotted using logarithmic scales. This analysis shows that, while spectral peaks at some orbital frequencies are indeed present in the data, they account for no more than 1.4 percent of the observed variance. The variance density of the temperature time series varies inversely as the square of the frequency, indicating that it is primarily a random walk phenomenon and stochastic in nature, rather than deterministic as would be the case if it were driven by orbital effects. Rapid warmings during the most recent glaciation known as Dansgaard-Oeschger events correspond closely to changes in ^{10}Be flux, suggesting that their origin lies outside the climate system.

A Re-examination of Ice Age Time Series

Introduction

Although Milankovic appears to have arrived at the theory of radiative forcing of climate by orbital variations as early as 1912, his theory was not published until 1920. A definitive statement of the theory appears in Milankovic (1941).

The theory proposes that variations in solar insolation arriving at critical Northern Hemisphere latitudes influence the formation and decay of the Arctic ice mass. These variations are due, in turn, to variations in the eccentricity and obliquity of the Earth in its orbit around the Sun together with coincidence of its axial precession with aphelion or perihelion. Eccentricity and obliquity are believed to generate periods of 100 and 42 ky respectively, while precession is believed to give rise to a period of ~23 ky.

As more deep sea sediment records became available, Hays, Imbrie and Shackleton (1976), using a spectral methodology due to Blackman and Tukey (1958), demonstrated the existence of spectral peaks in sediment time series at frequencies matching these frequencies. Since then the theory of climate forcing by solar insolation variations has become well established in the literature.

There are, however, some issues which are not completely resolved by the theory. Chief among these is the existence or otherwise of the eccentricity peak at 100 ky. This is the

major peak in the spectra of most Pleistocene time-series, and the rapid warmings which recur at this time scale known as ice age “Terminations” are the most obvious feature of such time series when they are displayed in the time domain. Furthermore older ice core data shows that the sequence of Terminations only commenced relatively recently, after 430 ky BP, known as the Mid-Pleistocene Revolution or Mid-Brunhes Event (MBE), see for example Maslin and Ridgwell (2005). Of most concern is the fact that, although this so-called “eccentricity cycle” predominates in the ice-core proxy records it is only a very small effect astronomically and leads to solar insolation changes which are more than an order of magnitude smaller than those due to obliquity and precession. So far no-one has put forward a convincing model to account for this anomaly.

Since the key paper by Hays *et al*, two important improvements in technology have occurred. On the one hand excellent ice core data from Vostok and EPICA Dome C have become available (Jouzel et al, 2007). On the other, the method of spectral analysis based on use of the Fast Fourier Transform (Cooley and Tukey, 1965) has come into widespread use. Not only do ice-cores offer better temporal resolution than do deep sea sediments, but their absolute time scales can be more precisely dated by comparison with geological markers such as volcanic eruptions. Variance density spectra computed using the FFT have superior frequency resolution compared to spectra estimated using the Blackman and Tukey method and lend themselves more readily to statistical testing.

Time Series and Spectra

Here, the validity of the orbital forcing hypothesis is tested by examining ΔT data derived from EPICA Dome C ice cores (Jouzel *et al, loc. cit.*) covering the period from ~460 ky to the present. Earlier data were ignored because of lower sampling rates and because the obvious discontinuity which occurred at the MBE precludes any assumption of stationarity. The EDC3 timescale was used.

By definition, a time series (or "random data sequence") comprises a sequence of quantities sampled at equal intervals of time. Typically, as a result of ice flow behaviour, more recent ice core data from near the surface are sampled much more densely in time than are deeper older data. This renders them unsuitable for processing as they stand because statistics would be biased toward the more densely sampled data.

Therefore a uniformly sampled time series was constructed by dividing the interval from the present to 461 ky BP into 512 intervals each 900 years in length. The values of all the data points lying within each interval were then averaged and the mean assigned to the mid-time of the interval. The number of intervals was selected to be a power of two for FFT purposes and the 900-year interval length was chosen to be sufficient to encompass at least one data point in each interval. The time series derived in this way is shown as curve "A" in Figure 1.

Also shown in Figure 1 are time series of computed integrated insolation energy values for Latitude 60^{o} North. Curve "B" is due to Berger (1992), and Curve "C" is due to Huybers and Eisenman (2006).

Variance density spectra for these three time series are shown plotted using logarithmic scales in Figure 2. Each spectral estimate is the squared modulus of the Fourier transform of the time series. No smoothing or windowing was carried out in either the time domain or the frequency domain.

In Figure 2, "A" is the spectrum of the ice core time series shown in Figure 1, while "B" and "C" are the spectra of the insolation time series. Frequencies of major peaks in the insolation spectra are shown by the vertical dashed lines labeled "a", "b", "c", "d" and "e". Peaks "a", "c" and "e" are the frequencies due to the eccentricity, obliquity and precession of the earth in it orbit. Peaks "b" and "d" appear only in the insolation data of Huybers and Eisenman. Details are listed in Table 1.

The dotted line in Figure 2 shows the locus of an f^{-2} spectrum.

Stochastic and Deterministic

According to the Wold Decomposition Theorem (Wold, 1954) any stationary time series can be expressed as the sum of a stochastic component and a linear deterministic component. A stochastic time series is one for which, at any given time, future terms cannot be predicted precisely and are governed by the laws of probability. A

deterministic sequence is one in which future values are completely determined by past values. These concepts are reviewed by Mandic *et al* (2008).

In Figure 1 time series “B” and “C” are known *a priori* to be deterministic since they are the outcome of calculations in celestial mechanics. Their population spectra will therefore consist of lines or delta functions corresponding to sinusoids in the time domain. The peaks in the spectral estimates, “B” and “C” in Figure 2, are finite, because these are obtained from samples of finite length in the time domain. In spectral estimation, the delta functions of the population spectrum are always degraded because they are convoluted with the Fourier transform of the finite data window; the longer the sample length, the narrower the peak becomes in the spectral estimate.

On the other hand, a stochastic process has a population spectrum which is continuous because it is the Fourier transform of the autocorrelation function, which tends to zero as the correlation lag tends to infinity. The spectral estimate of any sample of finite length from a stochastic sequence is always degraded by noise. Each ordinate, S(f), is the sum of the squares of the real and imaginary parts of the Fourier terms of the entire sample. By the central limit theorem these can be assumed to be Gaussian, so S(f) is a random variable which has a χ^2 distribution with 2 degrees of freedom. Such a spectral estimate always looks very noisy to the naked eye. It can, if needed, be smoothed by averaging neighbouring ordinates, so increasing the number of degrees of freedom and reducing the variance of the noise. There would, of course, be a corresponding reduction in frequency resolution.

The spectral estimate of the ice core proxy temperature time series, “A” in Figure 2, looks like a noisy straight line with slope = -2, with the peaks of interest occurring at the low frequency end, i.e. it is predominantly “red” noise, although there is the possibility of significant peaks at the various orbital frequencies. Such a linear trend on a log-log graph implies that there is a power law relationship between spectral density, S , and frequency, of the form

$$S(f) = Af^{-n}$$

where A is a constant, and the index, $n = 2$ in this case.

In many areas of physics, spectra are displayed on logarithmic scales to test for such power law behaviour. Power laws are widely used to test theories about underlying physical mechanisms. The value of the index, *n*, is crucial in this process. The physical implications of this inverse square power law will be discussed further below.

More importantly, it is the fact that there is a strong linear trend in the spectral estimate that is significant here. Such a linear trend indicates that the data sequence is stochastic in nature, i.e. that it is governed by the laws of probability. The spectrum of a purely deterministic time series would exhibit narrow peaks as do the insolation spectra, B and C of Figure 2. Even a chaotic data sequence would not give rise to a linear spectrum such as curve A in Figure 2. Nevertheless there remains the possibility that the sequence is a

mixture of cyclically deterministic and stochastic components. An upper limit on the contribution of the cyclic components needs to be found.

Whitening the Spectral Estimate

Spectral analysis is based on the "Power" Theorem of Fourier transforms, viz.: that the variance of the Fourier transform is equal to the variance of the original time series. Thus the spectrum reveals how the variance or "power" is distributed among frequencies. This concept can be generalized. Here we want to know how much variance is contained in the red noise spectrum, how much is contained in the orbital peaks and how much remains as remnant white noise.

One approach is to assume that the time series in question is the outcome of a wide-sense stationary process. The given time series can be envisaged as one of an ensemble of statistically similar time series each satisfying the same internal laws. The ensemble mean and variance are assumed to be independent of time, i.e. the series is assumed to be "wide-sense" stationary.

With little loss of generality, we shall further assume the time series is the outcome of an autoregressive random process, $\{X_t\}$, of finite order, ν, given by

$$X_t = \sum_{i=1}^{\nu} a_i x_{t-i} + \xi_t$$

where as a consequence of stationarity, a_i, are constants which are independent of time, and X_t and ξ_t are random variables, x_t is the realization of X_t at time t (an integer). The υ prediction coefficients, a_i, can be estimated from the data. The residual sequence, $\{\xi_t\}$, is assumed to be un-self-correlated or white noise with zero mean and constant variance. It is not necessarily Gaussian.

Once the regression coefficients have been estimated, the variance of the residuals or "prediction error power", P_ν, can be estimated from the data via

$$\hat{P}_\nu = \left(\sum_{t=1}^{N-\nu} (x_t - \sum_{i=1}^{\nu} \hat{a}_i x_{t-i}) \right)^2 = \left(\sum_{t=1}^{N-\nu} (\sum_{j=0}^{\nu} \hat{\gamma}_j x_{t-j}) \right)^2$$

where N is the length of the data sequence, and the "prediction error filter" or "PEF" coefficients, $\{\hat{\gamma}_j\}$, are given by $\hat{\gamma}_0 = 1$ and $\hat{\gamma}_i = -\hat{a}_i$ for $i = 1,...,\nu$, and the coefficients $\hat{a}_i$ have themselves been estimated from the data by the least squares method, i.e. by minimizing $\hat{P}_\nu$. The carat indicates numerical values that have been estimated from the data.

Comparison of the prediction error power estimate, $\hat{P}_\nu$, with the initial variance reveals how much of the latter can be accounted for by the regression process. In the extreme case, when P_ν is zero, each member of the sequence can be precisely predicted in terms of previous values of the sequence, and so the sequence is deterministic.

In the present case, because the slope of the spectral estimate is -2, we know from Fourier theory that the spectrum may be whitened by differentiating, or, in the discrete case, by taking first differences. This is equivalent to setting $\nu = 1$ and $\gamma_1 = -1$, so that a residual sequence, $\{y_t\}$, is generated by

$$y_t = x_t - x_{t-1} \qquad \text{for } t = 2,..., N$$

where the sequence $\{x_t\}$ is the time series of sampled ice core proxy temperatures shown as curve A in Figure 1.

The variance spectrum of $\{y_t\}$ is shown in Figure 3, where the labels indicate the same frequencies as in Figure 2. The spectrum is now nearly white (i.e. flat). The variance density spectrum of an un-self-correlated time series, i.e. of white noise, is flat, and each ordinate has a χ^2 distribution with 2 degrees of freedom as discussed above. Under the null hypothesis that the sequence of first differences is such a white noise sequence, confidence limits can be drawn. The mean, and upper and lower 95% and 99% confidence limits, are shown by the dashed lines in Figure 3.

Only peaks “c” and “e” are significant at the 99% level and peak “d” is significant at the 95% level. The so called “eccentricity peak” at “a” is not significant at all.

In addition the entire spectrum can be tested for whiteness using the Kolmogorov-Smirnov test. If the sequence of first differences is white then the cumulative distribution

of ordinates in the spectrum should closely resemble the cumulative χ^2 distribution. The KS parameter, D, was found to be 0.103, giving a probability of 0.0088. This means that under the null hypothesis that the sequence of first differences is white, the probability of a D value as large as this occurring by chance alone is 0.0088, i.e. the hypothesis can be rejected at the 99% level, and we can be confident that the sequence of first differences is not truly white. Thus statistical testing shows that the peaks are indeed real and not just the outcome of a random process. They are real, but how important are they?

The sequence, $\{y_t\}$, can be further whitened by using the conventional method of estimating the PEF coefficients, $\{\hat{\gamma}_j\}$, from the data, and using them to generate a second sequence of residuals, $\{z_t\}$, where

$$z_t = \sum_{i=0}^{\nu} \hat{\gamma}_i y_{t-i} \qquad \text{for } t = \nu + 2,..., N$$

The number of regression coefficients or "order" of the process, ν, is to some extent arbitrary. The correct choice of this parameter has been the subject of much discussion in the literature, particularly in the context of the Maximum Entropy Method of spectral estimation. Here it was chosen as the smallest value which would render each of the peaks "a", ...,"e" non-significant at the 95% level, which was $\nu = 65$. The use of such a large number of regression parameters for a sequence of only 512 terms would not normally be regarded as good statistical practice (see, for example, Reid, 1979). However, in this case the coefficient estimates themselves are not being used to estimate

a Maximum Entropy spectrum. Rather we are merely seeking to determine how much of the variance is associated with the statistically significant peaks.

The variance spectrum of the residual sequence, $\{z_t\}$, is shown in Figure 4. The orbital peaks are either non-significant or barely significant at the 95% level. The KS-test D statistic was 0.036 and its probability 0.88, indicating that this sequence is white, i.e. it is not significantly non-white.

The variances of the initial sequence, $\{x_t\}$, and the residual sequences, $\{y_t\}$ and $\{z_t\}$, are shown in Table 2.

The variance density spectra of Figures 2A, 3 and 4 together with the residual variances listed in Table 2 serve to demonstrate how much of the initial variance is associated with each component of the initial temperature proxy time series. Nearly 95 percent of the observed variance is associated with the "redness" of the original series indicating that the power law property is the most important aspect of the time series. When cyclic or quasi-cyclic components are further removed by filtering with a prediction error filter derived from the data, 4 percent of the variance still remains, indicating that these components contribute at most 1.36 percent of the variance. Note that this figure represents an upper limit on the cyclical components of the time series. Filtering with a PEF must always result in some reduction in variance even if no cyclic components were present initially.

The Time Domain

The previous section relates to a frequency domain description of the data. What are the time domain effects of these two filters?

The three data sequences $\{x_t\}$, $\{y_t\}$ and $\{z_t\}$ are shown plotted in Figure 5 in the time domain. Of particular interest is the sequence of first differences, the middle curve, $\{y_t\}$, which is the residual after the inverse square frequency trend has been removed but in which all other influences remain. The mean and $\pm 2\sigma$ values are shown as horizontal dashed lines. Five strong peaks are evident at the times of the five glacial terminations. The peaks are centred at the times listed in Table 3, and are marked by the vertical dashed lines in Figure 1 and Figure 5. Not only do these 5 peaks exceed the upper 2σ value, but in each case several adjacent values are high. So these peaks are indeed significant. Note that although there is a similar first difference peak associated with the termination-like behavior near 220 ky BP in Figure 5 the peak is not as large as the other 5 peaks.

The probability frequency density distribution of the $\{y_t\}$ sequence is shown in Figure 6. Also shown is a Gaussian curve with the same mean and standard deviation. It can be seen that the frequency distribution of $\{y_t\}$ is not Gaussian and is skewed; the spread of values greater than the mode is clearly greater than the spread of values smaller than the mode.

A stochastic process having an inverse square law red spectrum such as curve A of Figure 2 is known as random walk process, and is analogous to the Brownian motion of a

large particle interacting with an ensemble of much smaller particles. Such a climate system was described in theoretical terms by Hasselmann (1976) and applied by Frankignoul and Hasselmann (1977) to sea surface temperatures in mid-ocean regions. In his paper, Hasselmann emphasized the requirement that the system be characterized by two different response times. In the present work, the shorter response time applies to temperature variations which are more rapid than the 900 year sampling period of the sub-sampled time series, $\{x_t\}$. At shorter sampling times where the data density permits, as in the more recent, shallower ice cores, the spectral estimate was found to be almost white in accordance with Hasselmann's model.

The model requires an integrator analogous to the single massive particle of Brownian motion. In Frankignoul and Hasselmann's paper the integrator is the heat capacity or "thermal mass" of the ocean itself. At the longer time scales discussed here, an integrator with a much longer time-constant is required. There can be little doubt that this is the Northern Hemisphere ice sheet. The asymmetry of the density distribution shown in Figure 6 indicates that the rate of increase of temperature, and hence the rate of decrease of ice-sheet volume, tends to be more rapid than the rate of decrease of temperature and increase of ice sheet volume. In fact, the ice sheet appears to collapse dramatically at each Termination, each of which lasts for only a few thousand years. Various mechanisms have been proposed for this ice sheet collapse. These are reviewed by Imbrie et al (1993) and will not be discussed further here. All such proposed mechanisms are internal to the climate system.

The significance of the sequence of first differences is its skewed distribution, and the occurrence of 5 short impulses coincident with glacial terminations. The times of occurrence of these terminations are listed in Table 3. The average separation of these impulses in time is 103 ky, so they approximate the putative 100 ky “eccentricity peak”. They are clearly impulsive and non-sinusoidal in nature. However, the terminations recur at time intervals which are close to the 4th (92 ky) and 5th (115 ky) subharmonics of the 23 ky precession fluctuation (Table 3) also. This subharmonic relationship is clear to the naked eye in Figure 1

Note that the 5 peaks corresponding to the 5 terminations are no longer present in the bottom time series of Figure 5. This time series was derived by filtering the sequence of first differences with the prediction error filter. This filter removed the “orbital” frequency peaks in the frequency domain and the 5 termination impulses in the time domain. This indicates that these orbital frequency peaks are no more than a frequency domain effect of the presence of these impulses in the time domain. These 5 peaks together with the 220 KY BP peak are related to the 4th and 5th subharmonics of the eccentricity frequency. There is little evidence in the time domain for an obliquity peak at 41 ky. The very small upper limit that has been placed on the variance associated with the orbital frequencies suggests that insolation variations act as no more than a fortuitous trigger of ice age terminations which would have occurred anyway. However this sensitivity to a small triggering signal, if it is real, does suggest that the sequence of ice ages and interglacials is driven by forcings internal to the climate system. Visual examination of the temperature data displayed in Figures 1 and 5 suggests a system

oscillating between two meta-stable states as the Northern Hemisphere ice sheet builds up and then collapses during terminations.

Beryllium 10 concentration and Dansgaard-Oeschger Events

However the steady build up and sudden decay of the ice sheet on a time scale of 90 to 115 years may not be sufficient to account for temperature excursions which occur on other times scales. With this in mind it is worth looking at Beryllium 10 in ice cores. Beryllium 10 is produced in the stratosphere by collision of cosmic rays with atmospheric nitrogen atoms. Its production rate is therefore controlled by the primary cosmic ray intensity and by solar, extra-solar and geomagnetic modulations of that intensity, all of which processes lie outside of the climate system. Hence correlation of ^{10}Be data with proxy temperature could become a powerful tool in determining what forcings might be active in controlling global climate at 10 - 100ky time scales.

Some care must be taken however. Cosmic ray and geomagnetic effects control the flux of ^{10}Be whereas it is the *in situ* concentration of ^{10}Be which is reported in ice core data.

This difficulty is easily remedied. The flux (in atoms.m^{-2}.year^{-1}) is given by the concentration (in atoms.m^{-3}) multiplied by the snow accumulation rate (in m.year^{-1}). All that is required is accumulation data with which to correct ^{10}Be concentration to yield ^{10}Be flux, preferably from the same ice cores to avoid errors due to variations in time scales between sites. Both such data sequences are available fromGISP2.

Figure 7 shows ^{10}Be concentration (Finkel; 1997), accumulation rate (Alley, 2004) and computed ^{10}Be flux at GISP2, Greenland for the period from 40 ky to 3 ky BP. The values of ^{10}Be flux shown in the lowest curve are the products of corresponding values of concentration and accumulation rate displayed as the upper two curves. Concentration and flux curves are inverted for ease of comparison with temperature.

Figure 8 shows Δ^{18}O proxy temperature from GISP2 (Alley, 2004) alongside the corresponding ^{10}Be flux from GISP2 already displayed in Figure 7.

The upper curve shows the temperature of central Greenland from 40 ky BP to the present day. The upward trend in temperature from 17ky BP to 11 ky BP is the most recent termination. The downward trend near 13 ky BP is termed the Younger Dryas (YD). The upward going spikes in the temperature curve between 38 and 23 ky BP are known as Dansgaard-Oeschger (DO) events.

Like the terminations that can be seen in Figure 5 on a longer time scale, the DO events in Figure 8 are clearly impulsive and random in nature, with rapid onset and slower decay.

The ^{10}Be flux data displayed in Figure 8, show a striking resemblance to the temperature data in the period 38 to 23 ky BP, i.e. to the DO events. There is a good correspondence between seven major peaks in this part of these records. Figure 7 indicates that this

cannot be accounted for by variations in the ^{10}Be accumulation rate, which is almost constant for this period.

On the other hand, there is little relationship between ^{10}Be flux and temperature during the period of the termination and the YD. The double spike in ^{10}Be flux at 14 ky BP may well be an artifact brought about by smoothing of the accumulation data.

The importance of the resemblance between ^{10}Be flux and temperature during the interval of DO events cannot be overstated. It is strong evidence that the forcing which drives the DO events almost certainly comes from outside the climate system.

On the other hand, the most recent termination, and the YD, show no such correspondence, implying that they may have a different origin. Firestone et al (2007) have found evidence that the YD at 12.9 ky BP was caused by an extra-terrestrial impact event leading to the extinction of many mammalian taxa. Extinct Pleistocene megafauna are found before this date but not after. They point out that although abrupt coolings of similar magnitudes to the YD occurred often during the past 80 ky, none are associated with similar major extinctions. Whatever the cause of the YD, this is evidence that it was indeed different in kind to the DO events.

Conclusions

The EPICA Dome C proxy temperature time series obtained by sampling every 900 years from 461 ky BP to the present exhibits a power law spectrum with an index of -2.

It follows that global temperature as recorded in these ice cores is primarily stochastic rather than deterministic in character, and is a random walk process.

The spectrum of the sequence of first differences is almost flat, but with statistically significant peaks at periods of 41, 28.6 and 23 ky. There is no significant peak near the orbital period of 100 ky.

Whitening the spectrum by taking first differences removed 94.6 percent of the variance.

Examination of the sequence of first differences in the time domain reveals 5 short impulses corresponding to rapid warming at terminations.

Further whitening by convoluting with a prediction error filter estimated from the data showed that orbital forcing accounted for less than 1.4 percent of the variance of the original time series.

It follows that insolation changes due to orbital variations cannot reasonably be assumed to drive the sequence of ice ages and interglacials. At best insolation changes may act as a trigger or pacemaker at subharmonics of the precession frequency of 23 ky. A sequence of ice ages and interglacials may well have occurred had there been no orbital variations but this synchronicity suggests that terminations may originate within the climate system.

Beryllium 10 flux data, from GISP2 in Central Greenland, strongly suggest that some excursions in temperature known as Dansgaard-Oeschger events are driven by forcings which come from outside the climate system, either from abrupt changes in energy flux from the sun, or solar or extra-solar modulation of cosmic rays, or because of instabilities in the earth's mantle which both warm the atmosphere and modulate ^{10}Be flux via geomagnetic field variations.

The rapid cooling known as the Younger Dryas belongs in a third category in that it neither corresponds to major changes in ^{10}Be flux nor does it correspond to a subharmonic of precessional isolation variations.

Acknowledgements

I would like to thank Stuart Godfrey, Michael Stein and Ken McCracken for helpful advice and comment during the preparation of this paper.

References

Alley, R.B.. (2004)."GISP2 Ice Core Temperature and Accumulation Data." *IGBP PAGES/World Data Center for Paleoclimatology Data Contribution Series* #2004-013. NOAA/NGDC Paleoclimatology Program, Boulder CO, USA. ftp://ftp.ncdc.noaa.gov/pub/data/paleo/icecore/greenland/summit/gisp2/isotopes/gisp2_temp_accum_alley2000.txt

Berger, A. (1992) “Orbital Variations and Insolation Database”. IGBP PAGES/World Data Center for Paleoclimatology Data Contribution Series # 92-007. NOAA/NGDC Paleoclimatology Program, Boulder CO, USA.

Blackman, R.B. and J.W. Tukey (1958) *The Measurement of Power Spectra from the Point of View of Communication Engineering*. Dover, New York.

Cooley, J. W., and J. W. Tukey (1965) "An algorithm for the machine calculation of complex Fourier series," *Math. Comput.* **19**, 297–301. doi:10.2307/2003354

Finkel, R.C., and K. Nishiizumi. (1997). “Beryllium 10 concentrations in the Greenland Ice Sheet Project 2 ice core from 3-40 ka.” *J. Geophys. Res.* 102:26699-26706. ftp://ftp.ncdc.noaa.gov/pub/data/paleo/icecore/greenland/summit/gisp2/cosmoiso/ber10.txt

Firestone, R.B., A. West, J. P. Kennett, L. Becker, T. E. Bunch, Z. S. Revay, P. H. Schultz, T. Belgya, D. J. Kennett, J. M. Erlandson, O. J. Dickenson, A. C. Goodyear, R. S. Harris, G. A. Howard, J. B. Kloosterman, P. Lechler, P. A. Mayewski, J. Montgomery, R. Poreda, T. Darrah, S. S. Que Hee, A. R. Smith, A. Stich, W. Topping, J. H. Wittke, and W. S. Wolbach (2007) “Evidence for an extraterrestrial impact 12,900 years ago that

contributed to the megafaunal extinctions and the Younger Dryas cooling", *Proc Natl Acad Sci* U S A. **104**(41): 16016–16021.

Frankignoul, C. and K. Hasselmann (1977) "Stochastic climate models, Part II Application to sea-surface temperature anomalies and thermocline variability". *Tellus* **29**, 4.

Hasselmann, K. (1976) "Stochastic climate models, Part I, Theory". *Tellus* **XXVIII**, 6.

Hays, D.J., J. Imbrie and N.J Shackleton (1976) "Variation in the Earth's Orbit: Pacemaker of the Ice Ages." *Science*, **194**, 4270, pp 1121-1132.

Huybers, P. and I. Eisenman, (2006). "Integrated Summer Insolation Calculations". IGBP PAGES/World Data Center for Paleoclimatology, Data Contribution Series # 2006-079. NOAA/NCDC Paleoclimatology Program, Boulder CO, USA. (ftp://ftp.ncdc.noaa.gov/pub/data/paleo/climate_forcing/orbital_variations/huybers2006insolation/huybers2006b.txt)

Imbrie, J. , Berger, A. , Boyle, E. A. , Clemens, S. C. , Duffy, A. , Howard, W. R. , Kukla, G. , Kutzbach, J. , Martinson, D. G. , McIntyre, A. , Mix, A. C. , Molfino, B. , Morley, J. J. , Peterson, L. C. , Pisias, N. G. , Prell, W. L. , Raymo, M. E. , Shackleton, N. J. & Toggweiler, J. R. (1993) "On the structure and origin of major glaciation cycles 2. The 100,000-year cycle". *Paleoceanography* **8 ,** 699–736 .

Jouzel, J., V. Masson-Delmotte, O. Cattani, G. Dreyfus, S. Falourd, G. Hoffmann, B. Minster, J. Nouet, J.M. Barnola, J. Chappellaz, H. Fischer, J.C. Gallet, S. Johnsen, M. Leuenberger, L. Loulergue, D. Luethi, H. Oerter, F. Parrenin, G. Raisbeck, D. Raynaud, A. Schilt, J. Schwander, E. Selmo, R. Souchez, R. Spahni, B. Stauffer, J.P. Steffensen, B. Stenni, T.F. Stocker, J.L. Tison, M. Werner, and E.W. Wolff. (2007) "Orbital and Millennial Antarctic Climate Variability over the Past 800,000 Years." *Science*, **317**, 5839, pp.793-797, (http://www.ncdc.noaa.gov/paleo/icecore/antarctica/domec/domec_epica_data.html)

Mandic, D.P., M. Chen. T. Gautama, M.M. Van Hulle and A. Costantinides. (2008). "On the characterization of the deterministic / stochastic and linear / non-linear nature of time series". *Proc. R. Soc*. **464**, 1141 -1160. doi:10.1098/rspa.2007.0154 (http://simone.neuro.kuleuven.be/marc/Proc_Roy_Soc_A_2008.pdf)

Maslin, M.A. and A.J. Ridgwell (2005) "Mid-Pleistocene Revolution and the "eccentricity myth". *Geological Society, London, Special Publications*; 2005; v. 247; p. 19-34; DOI: 10.1144/GSL.SP.2005.247.01.02

Milankovic, M. (1941) "Kanon der Erdbestrahlung und seine Anwendung auf das Eiszeitenproblem". *Koniglich Serbische Akademie*, Belgrade.

Reid, J.S. (1979) “Confidence Limits and Maximum Entropy Spectra”. *J. Geophys. Res*. **84**, A9 5289-5301

Steig, E.J., Brook, E.J., White, J.W.C., Sucher, C.M., Bender, M.L., Lehman, S.J., Morse, D.L., Waddington, E.D., Clow, G.D. (1998). “Synchronous climate changes in Antarctica and the North Atlantic”. *Science* **282** (5386): 92-95. (ftp://ftp.ncdc.noaa.gov/pub/data/paleo/icecore/antarctica/taylor/betd.txt)

Wold, H. (1954) *A Study in the Analysis of Stationary Time Series*, Second revised edition, with an Appendix on "Recent Developments in Time Series Analysis" by Peter Whittle. Almqvist and Wiksell Book Co., Uppsala.

Tables

Label	Description	Frequency (ky^{-1})	Period (ky)
a	Eccentricity	.01	100
b	Obliquity "sideband"?	.0185	54
c	Obliquity	.0244	41
d	Obliquity "sideband"?	.035	28.6
e	Precession	.043	23

Table 1. Frequencies and periods of insolation peaks illustrated in Figure 1.

Description	Symbol	Variance	Percentage Remaining	Percentage Difference
Initial sequence	$\{x_t\}$	10.63	100	
After differencing	$\{y_t\}$	0.57	5.38	94.62
After orbital peaks removed	$\{z_t\}$	0.43	4.02	1.36

Table 2. Proportion of variance associated with the three sequences shown in Figure 5.

Termination	t (ky BP)	Δt (ky)	average Δt (ky)
I	13		
II	131	118	
III	243	112	115
IV	337	94	
V	425	88	91

Table 3. The timing of 5 glacial terminations, t. Δt is the time difference between successive terminations. The leftmost column lists the averages of the long (I, II and III) and the short (III, IV and V) time differences

Diagrams

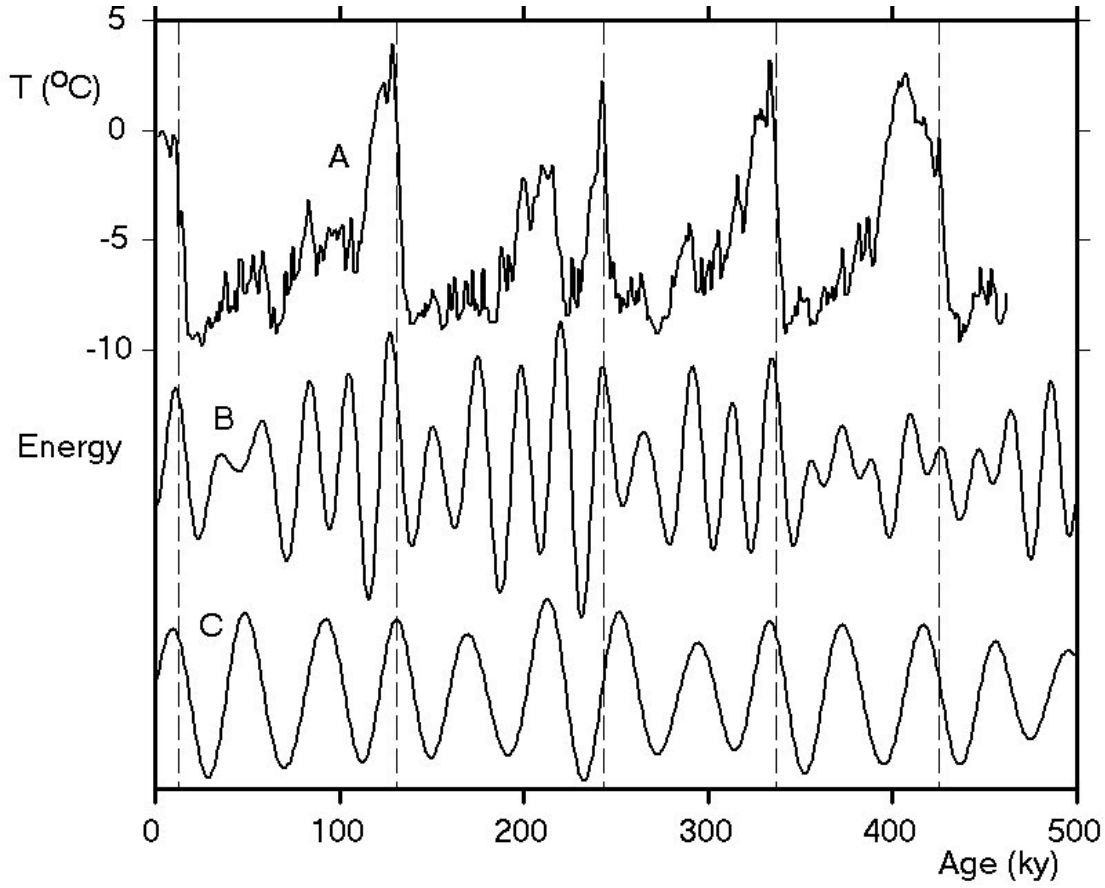

Figure 1. A. EPICA Dome C proxy temperatures after sampling at 0.9 ky intervals. B. Integrated solar insolation energy at 60° N due to Berger (1992). C. Integrated solar insolation energy at 60° N due to Huybers and Eisenman(2006).

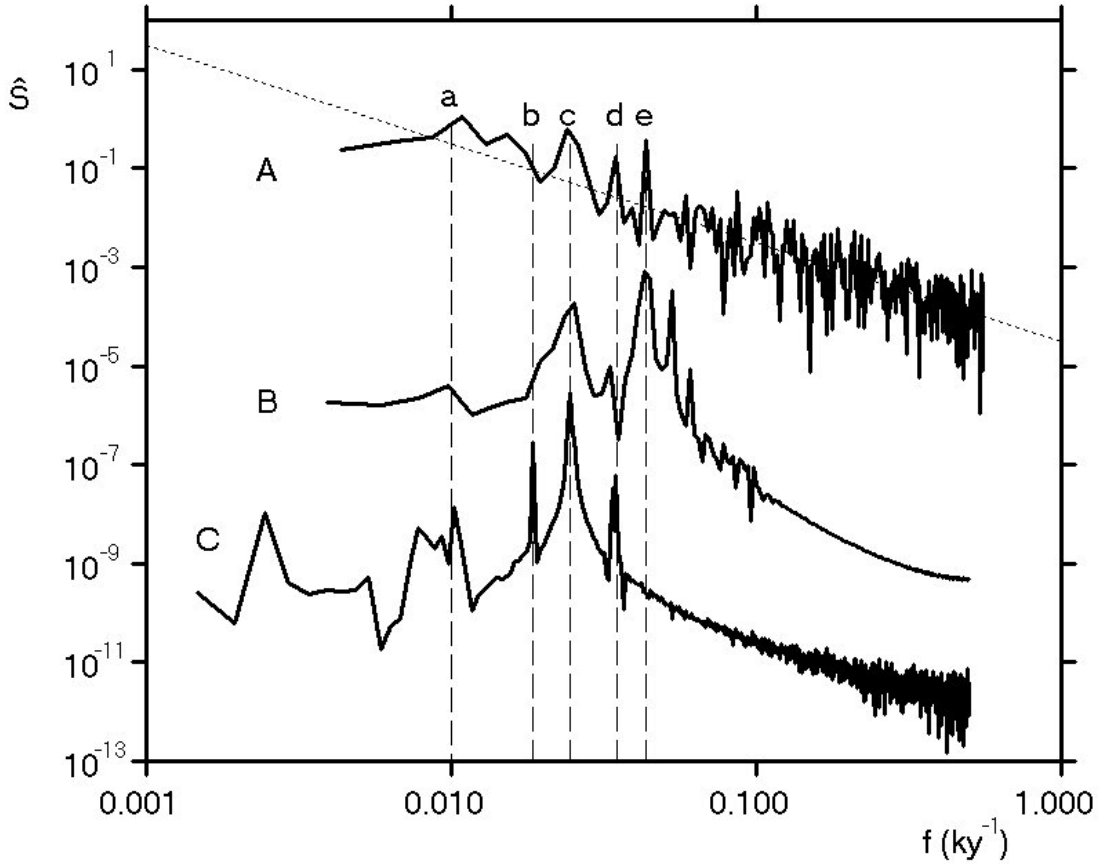

Figure 2. Variance density spectra of the time-series plotted in Figure 1 plotted using logarithmic scales. The dashed lines show the frequencies of the various peaks in insolation due to the Earth's orbital variations as listed in Table 1. "a" shows the frequency of the eccentricity peak, "c" the obliquity peak and "e" the peak due to the precession of the equinoxes. The dotted line is the locus of an f^{-2} power law spectrum.

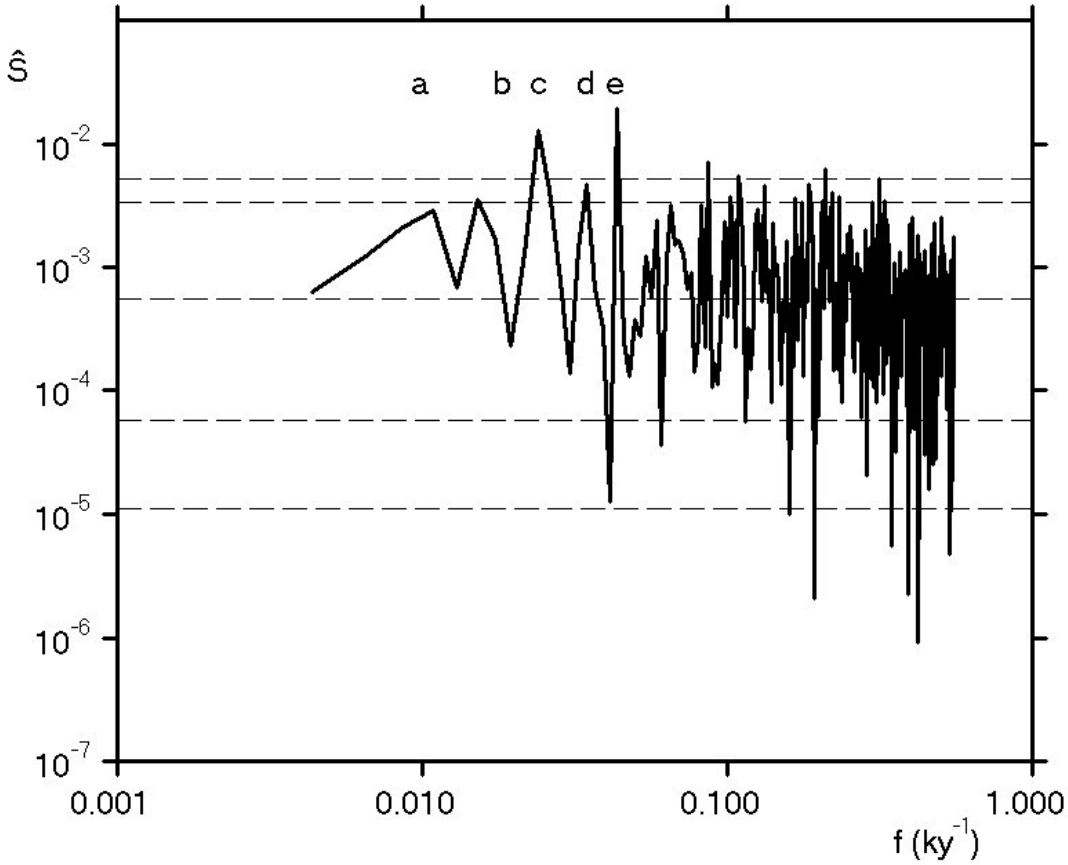

Figure 3. Variance density spectrum of the sequence of first differences of the temperature time-series shown in Figure 1. The labels "a", "b", "c", "d", and "e" depict the frequencies shown in Figure 2 and listed in Table 1. The dashed lines show the mean and the upper and lower 99 percent and 95 percent confidence limits.

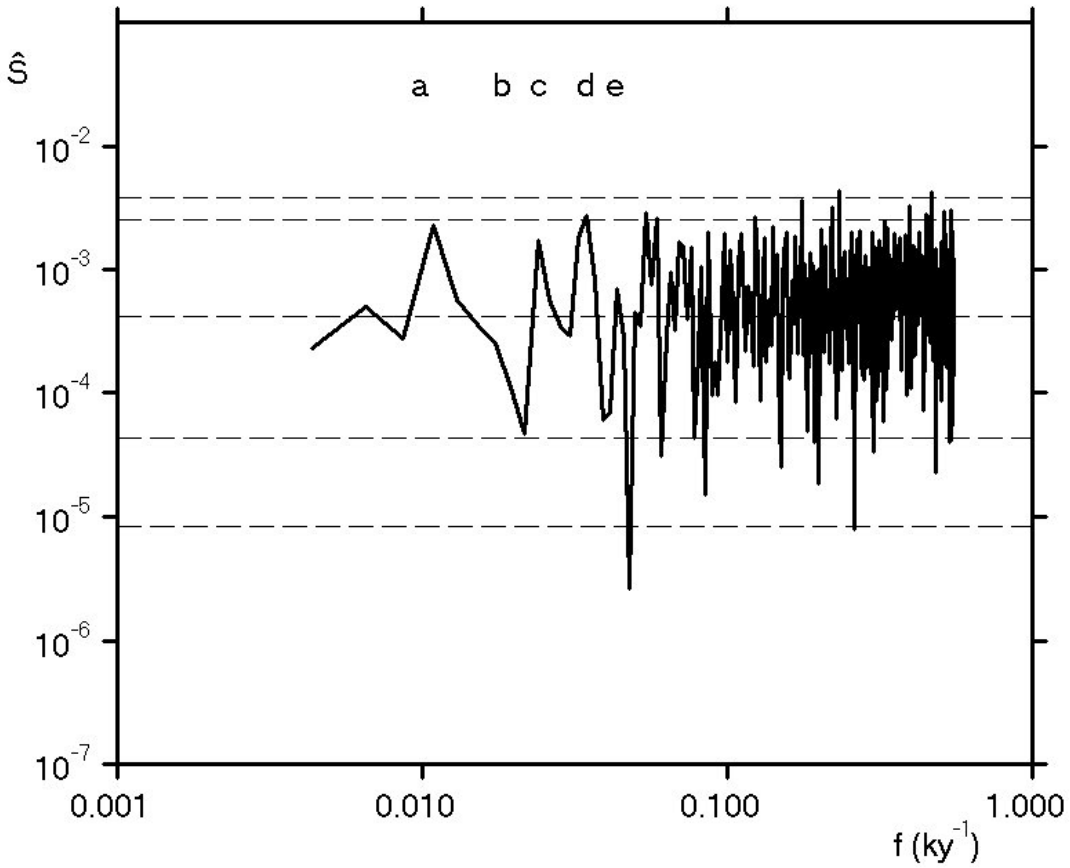

Figure 4. Variance density spectrum of the sequence of residuals following convolution of the first difference sequence with a 65-long sequence of PEF coefficients. The labels "a", "b", "c", "d", and "e" depict the frequencies shown in Figure 2 and listed in Table 1. The dashed lines show the mean and the upper and lower 99 percent and 95 percent confidence limits.

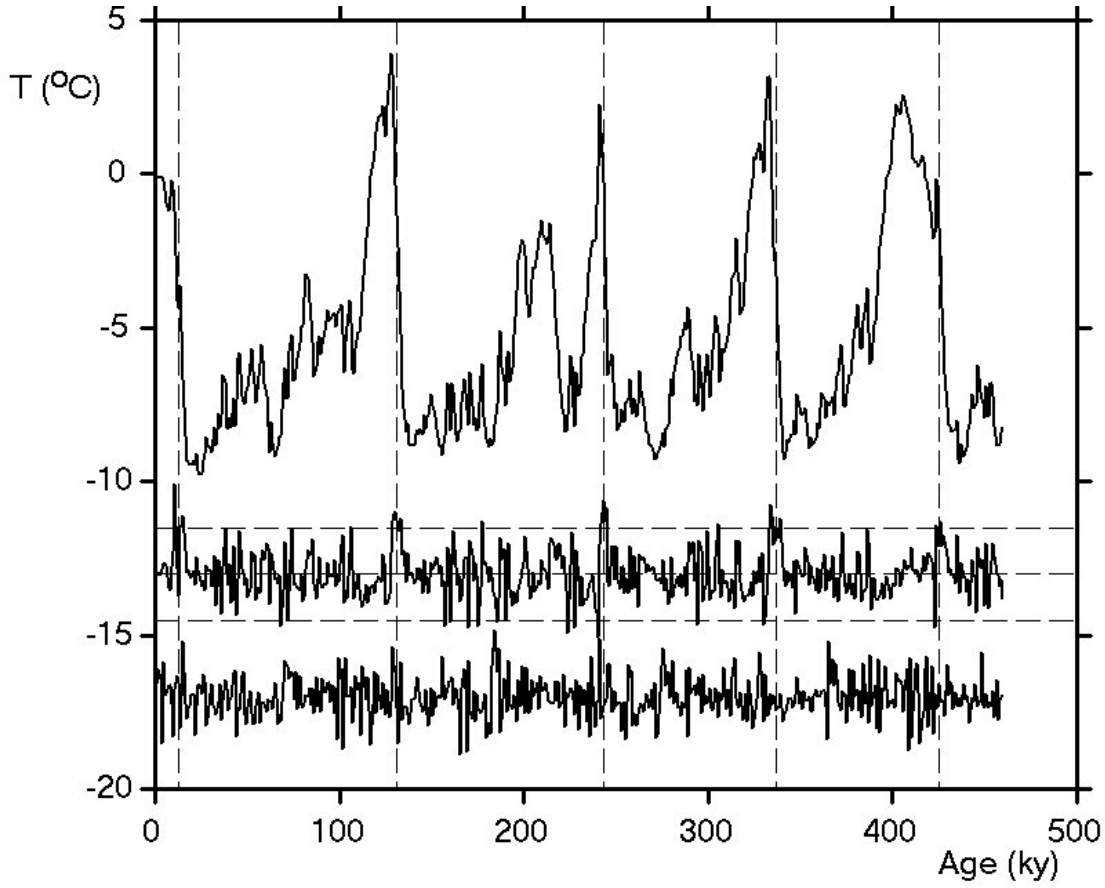

Figure 5. Upper curve: sequence of temperature differences from EPICA Dome C ice cores shown in Figure 1. Middle curve: sequence of first difference of the sequence of temperature differences (variance density spectrum shown in Figure 3). Lower curve: sequence of residuals obtained when the sequence of first differences is convoluted with the sequence of PEF coefficients. The horizontal dashed lines show the mean and the mean ±2σ range of the first difference sequence. The five vertical dashed lines show the times of impulsive warming ("Terminations").

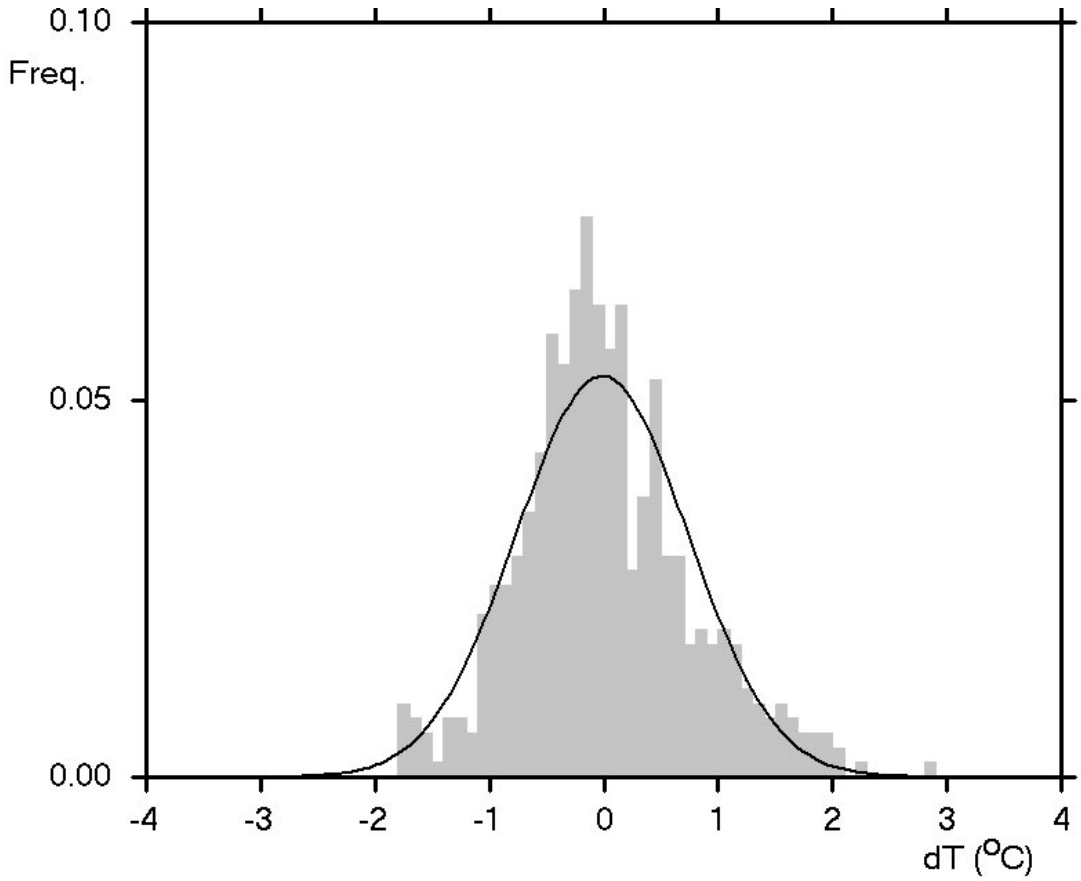

Figure 6. The histogram shows the frequency density of the distribution of values of the sequence of first differences shown in Figure 5. The continuous curve shows the Gaussian distribution with the same mean and standard deviation.

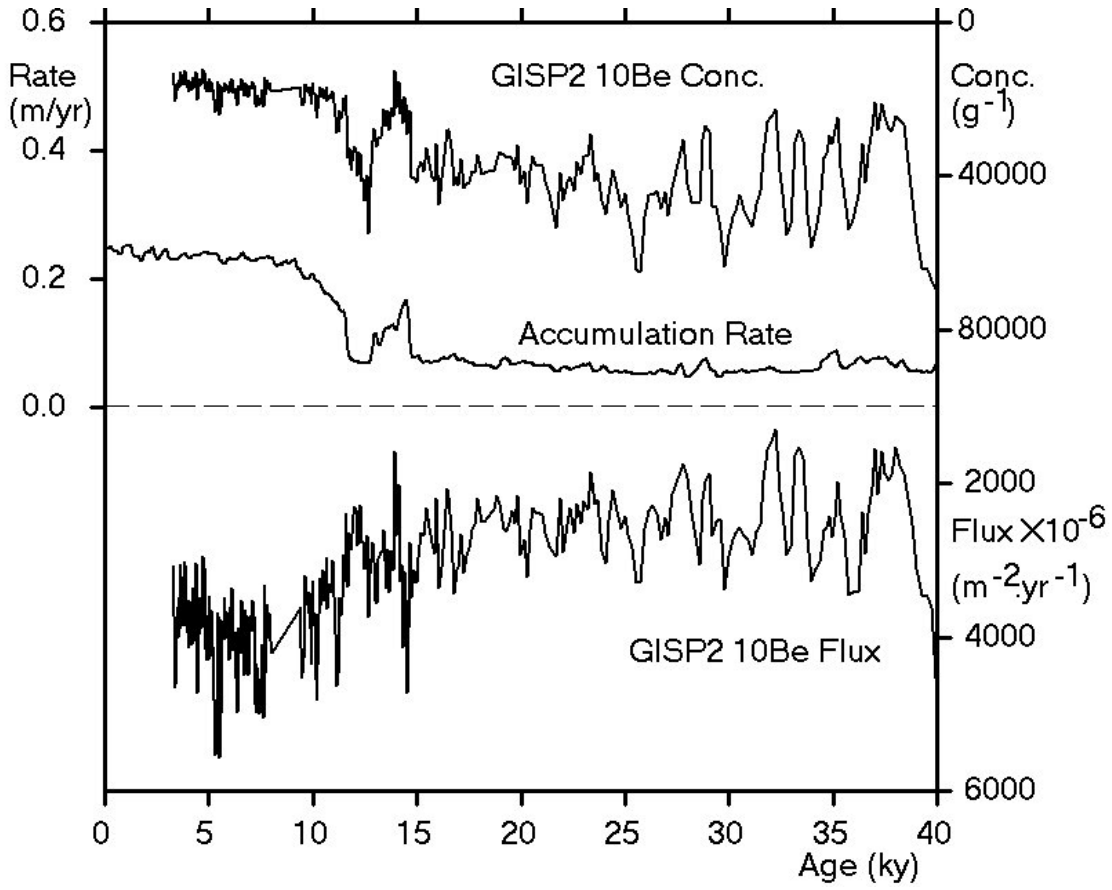

Figure 7. ^{10}Be concentration, accumulation rate and computed ^{10}Be flux at GISP2, Greenland for the period from 40 ky to 3 ky BP. The ^{10}Be flux is the product of the upper two curves. Concentration and flux curves are inverted for ease of comparison with temperature.

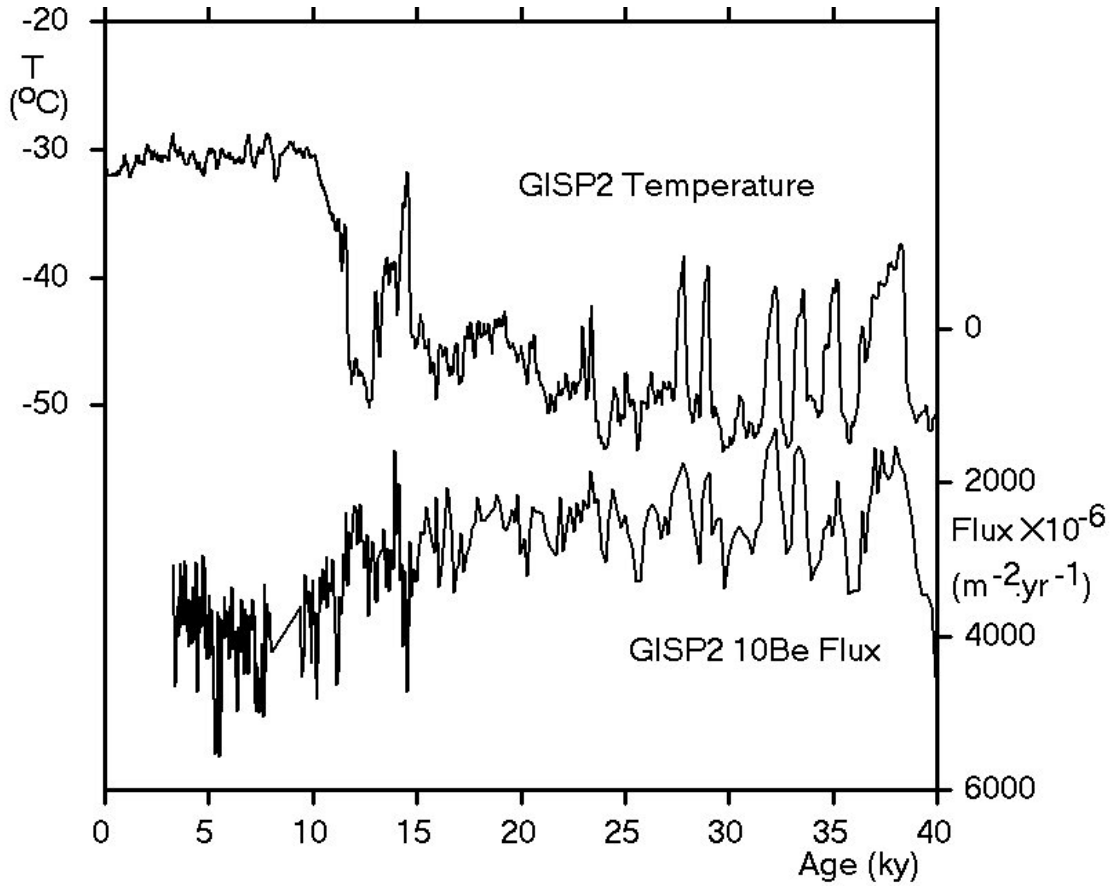

Figure 8. Δ^{18} **O proxy temperature from GISP2 and** ^{10} **Be flux from GISP2 as shown in Figure 7.**